

Growth of semi-coherent Ni and NiO dual-phase nanoparticles using hollow cathode sputtering

Sebastian Ekeroth  · Shuga Ikeda · Robert D. Boyd · Tetsuhide Shimizu · Ulf Helmersson

Received: 5 December 2018 / Accepted: 30 January 2019 / Published online: 13 February 2019
© The Author(s) 2019

Abstract Anisotropic heterogenous Ni/NiO nanoparticles with controlled compositions are grown using a high-power pulsed hollow cathode process. These novel particles can be tuned to consist of single-phase Ni via two-phase Ni/NiO to fully oxidized NiO, with a size range of 5–25 nm for individual crystals. A novelty of this approach is the ability to assemble multiple particles of Ni and NiO into a single complex structure, increasing the Ni-NiO interface density. This type of particle growth is not seen before and is explained to be due to the fact that the process operates in a single-step approach, where both Ni and O can arrive at the formed nanoparticle nuclei and aid in the continuous particle growth. The finished particle will then be a consequence of the initially formed crystal, as well as the arrival rate ratio of the two species. These particles hold great potential for applications in fields, such as electro- and photocatalysis, where the ability to control the level of oxidation and/or interface density is of great importance.

Keywords Ni · NiO · Anisotropic · Nanoparticles · Hollow cathode · Nanoparticle assembly

Electronic supplementary material The online version of this article (<https://doi.org/10.1007/s11051-019-4479-4>) contains supplementary material, which is available to authorized users.

S. Ekeroth (✉) · R. D. Boyd · U. Helmersson
Department of Physics, Chemistry and Biology, Linköping
Universitet, 58183 Linköping, Östergötland, Sweden
e-mail: sebastian.ekeroth@liu.se

S. Ikeda · T. Shimizu
Department of Intelligent Mechanical Systems, Tokyo
Metropolitan University, Tokyo, Japan

Introduction

Ni/NiO composite materials are of interest in a number of applications, including energy-related hydrogen evolution (Wang et al. 2017), lithium ion batteries (Bell et al. 2015), and supercapacitors (Liu et al. 2017). For the production of hydrogen, these materials display excellent catalytic behavior during electrocatalytic water splitting for the hydrogen evolution reaction (HER) (Gong et al. 2014). Here, Pt is regarded as state-of-the-art material and is often used as a benchmark (Cheng et al. 2016; Subbaraman et al. 2011; Yin et al. 2015); but because of its dearth in nature, other materials are needed (Yung et al. 2014). One alternative is Ni/NiO, where theoretical studies have identified active sites on Ni(111) near the interface of NiO that provides HER performance that can be equal or even higher than that of Pt (Pan and Zhou 2018). The existence of NiO shifts the d-states of surface Ni atoms down in energy and enhances the reactivity of the exposed Ni surface. This has been demonstrated experimentally using nanoparticles attached to a carbon nanotube network (Gong et al. 2014). Partly oxidized Ni nanoparticles can also be used for photocatalytic hydrogen generation (Yeh et al. 2017). Common to all of these applications, the partially oxidized nanoparticles display the best results. This means that to synthesize the “dual-phase” Ni/NiO material to perform at its best, it is important to be able to precisely control both the Ni/NiO composition and their amount of interfaces.

The Ni-O phase diagram is simple and consists only of two solid phases: fcc Ni and cubic (B1) NiO, where the fcc Ni lattice in NiO is 18% expanded as compared with

that in pure Ni. The solvability of O in the bulk of Ni is only 0.05 at.% even at 1000 °C (Park and Altstetter, 1987). However, in the near-surface region, considerable amount of O can be dissolved (Deckers et al. 1990). This has important consequences for the synthesis and structure evolution of nanoparticles of Ni and NiO in oxygen environments. This was described elegantly by Koga and Hirasawa (2013) in post-oxidation of spherical Ni nanoparticles into short NiO rods.

There are several different methods for producing Ni/NiO nanoparticles. For example, oxidizing pure Ni nanoparticles (Koga and Hirasawa 2013), or using chemical reactive processes to grow Ni (Gang Wu et al. 2010) or NiO (El-Kemary et al. 2013). A common issue is the difficulty in precisely controlling the level of oxidation of the nanoparticles (i.e., the relative composition of Ni and NiO) or to have a structure other than a metallic core and oxide shell in a single-step approach (Spadaro et al. 2015).

In this work, we demonstrate the ability to grow Ni/NiO nanoparticles with interconnected interfaces and how to tune their composition ranging from pure Ni to pure NiO by using a hollow cathode pulsed plasma process (Pilch et al. 2013). This allows the nucleation and growth of nanoparticles in a gas-phase environment that consists of sputtered vapor, as well as inert and reactive gases. Thus, the control of Ni to NiO ratio can be achieved during the growth of nanoparticles, by adjusting the flow of oxygen gas. In particular, we show that particles with several domains of interconnecting Ni-NiO can be created. Because of the wide range of particles achievable, there are many possible applications. In a separate work, not discussed here, we demonstrate one example of how these particles can be utilized. There, fully oxidized NiO particles are used as photoanodes for enhanced solar water splitting (Jian et al. 2019).

Experimental

Hollow cathode sputtering is used to synthesize the nanoparticles in a high vacuum chamber with a base pressure of 3×10^{-7} Torr (4×10^{-5} Pa). The cathode consists of a Ni tube with an internal diameter of 5 mm, a length of 54 mm, and a purity of 99.98%. The cathode is placed in a copper block for easy mounting on a water-cooled holder. The anode, consisting of a stainless steel ring 35 mm in diameter, is positioned 25 mm from the cathode exit. A cylindrical, stainless steel mesh cage with a

diameter of 85 mm and a length of 110 mm is placed covering the hollow cathode exit and the anode ring and contains an exit in the end opposing the hollow cathode. A substrate table, with the capacity to hold seven substrates, is positioned 20 mm outside the exit of the cage. Between the cage opening and the substrate table, a shutter is located to control the deposition of nanoparticles onto the substrates. A positive bias of 18 V is used to guide the negatively charged nanoparticles to the substrate. Ar with a purity of 99.9997% is used as the sputter gas, and it is fed through the cathode with a flow rate of 30 sccm throughout the experiments reported here. However, flow rates ranging 10–70 sccm were tested in order to optimize the shape and size of the particles. A reactive sputter gas, O₂, is let into the chamber approximately 30 cm downstream of the cathode. The O₂ gas is diluted with Ar gas to 99.5%, resulting in an effective O₂ flow ranging 0–0.08 sccm. A schematic drawing of the vacuum system can be seen in Fig. 1. To keep the working pressure fixed around 0.82 Torr (109 Pa), a throttle valve, mounted in front of the vacuum pump, is used. The pulsed electrical power is supplied to the cathode via a HiPSTER 1 pulsing unit (Ionautics AB) that is fed by a MDX-1K dc power supply (Advanced Energy). Pulsing frequencies from 300 to 1800 Hz were tested; but for the results presented here, the frequency is fixed to 1200 Hz, a frequency that produced the most uniform particles in terms of shape and size. Pulse width is also kept fixed at 80 μs, giving a duty cycle of 9.6%. The average current is kept at 140 mA, with an average power of ~50 W.

The particles were characterized using transmission electron microscopy (TEM). Prior to analysis, particles are deposited directly onto carbon-coated TEM grids with no additional sample preparation. All measurements are taken in a FEI Tecnai G2 operated at 200 kV. High-angle angular dark field (HAADF) and energy dispersive X-ray spectroscopy (EDS) are combined with scanning-TEM (STEM) analyses using an annular detector spanning an angular range from 80 to 260 mrad.

Results

Figure 2 shows TEM and STEM HAADF images of nanoparticles generated in the different oxygen environments. Common for all environments studied is a bimodal size distribution with small (~5 nm) and large (~25 nm) nanoparticles as well as, for higher oxidations, assemblies of nanoparticles. Images of these different

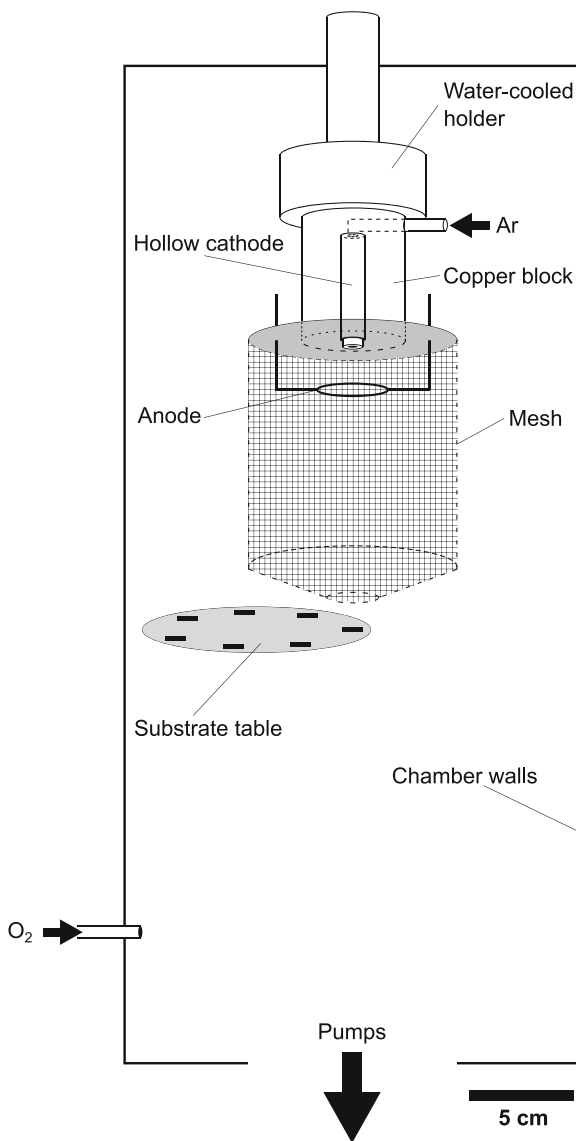


Fig. 1 Schematic drawing of the vacuum system to scale

particles and assemblies are arranged in rows of the figure, whereas the columns are associated with the different oxygen flows used. Each individual image is identified using matrix indices, such as Fig. 2n,m.

The first two columns, Fig. 2a,m and b,m, both illustrate essentially spherical particles synthesized using a pure Ar process and the lowest oxygen flow (0.02 sccm), respectively. Lattice parameter studies of the larger particles conclude that they consist of a Ni core. On the surface, there is a thin shell with a thickness of $\sim 1\text{--}2$ nm assumed to be NiO formed after exposing the pure Ni surface to air (Jesús et al. 1996). A rough estimate of the nanoparticle deposition rate gives a value

of totally 10^3 nanoparticles per square micrometer and minute with approximately the same number of small and large particles.

The third column, Fig. 2c,m, exemplifies particles grown adding 0.04 sccm of oxygen to the process. In this case, most of the nanoparticles consist of two domains, a spherical shaped Ni and a cubical shaped NiO, with crystal lattices oriented coherently between the two phases. This is seen in the TEM image in Fig. 2c,ii, which also shows Moiré fringes formed as the two crystal lattices overlaps in the image. The spacing between the Moiré fringes is ~ 1.0 nm, which corresponds to the expected value for Moiré patterns from two relaxed fcc lattices with cell parameters corresponding to that of Ni and NiO, 3.52 and 4.17 Å, respectively (Kittel 1996; Bartel and Morosin 1971). The alignment between the two different crystals is due to energy minimization forming a semi-coherent interface with misfit dislocation compensating for the difference in lattice parameter. On occasion, a smaller Ni domain is seen on the corner of a NiO domain, and two NiO domains will connect leading to a dumbbell-shaped structure.

For O_2 flow of 0.04 sccm and higher, an increasing fraction of the nanoparticles formed is assembled into larger structures consisting of several Ni and NiO crystals. This is illustrated in the fourth row, Fig. 2n,iv. Here, a few particles (2 to 5) are commonly observed in the assemblies, where the Ni and NiO crystals are of similar sizes as exemplified in Fig. 2c,iv. The two crystal types align coherently as can be seen in the lattice resolution TEM picture, Fig. 2c,v. In the STEM HAADF image, Fig. 2c,vi, it clearly shows that the spherical Ni crystals appear brighter (scatter more electrons) than the less-dense cubic NiO. The elemental compositions of the two different crystals are confirmed by STEM-EDS (see Fig. S1 of the Supplementary information).

Increasing the O_2 flow further to 0.06 sccm still yields two-phase nanoparticles but with an increasing fraction of the NiO phase. Small Ni domains, often several on each NiO crystal, are attached in corners or on the 100 faces of the NiO crystal, Fig. 2d,ii.

For the highest oxygen flow investigated, 0.08 sccm, the smaller sized particles become scarcer, and the larger 25-nm nanoparticles dominate. These nanoparticles consist of almost pure NiO, sometimes with small Ni domain precipitates on their surface. This can be seen in Fig. 2e,ii where the NiO nanoparticle has two 2–4-nm-sized Ni particles attached to the surface as revealed by the Moiré patterns generated.

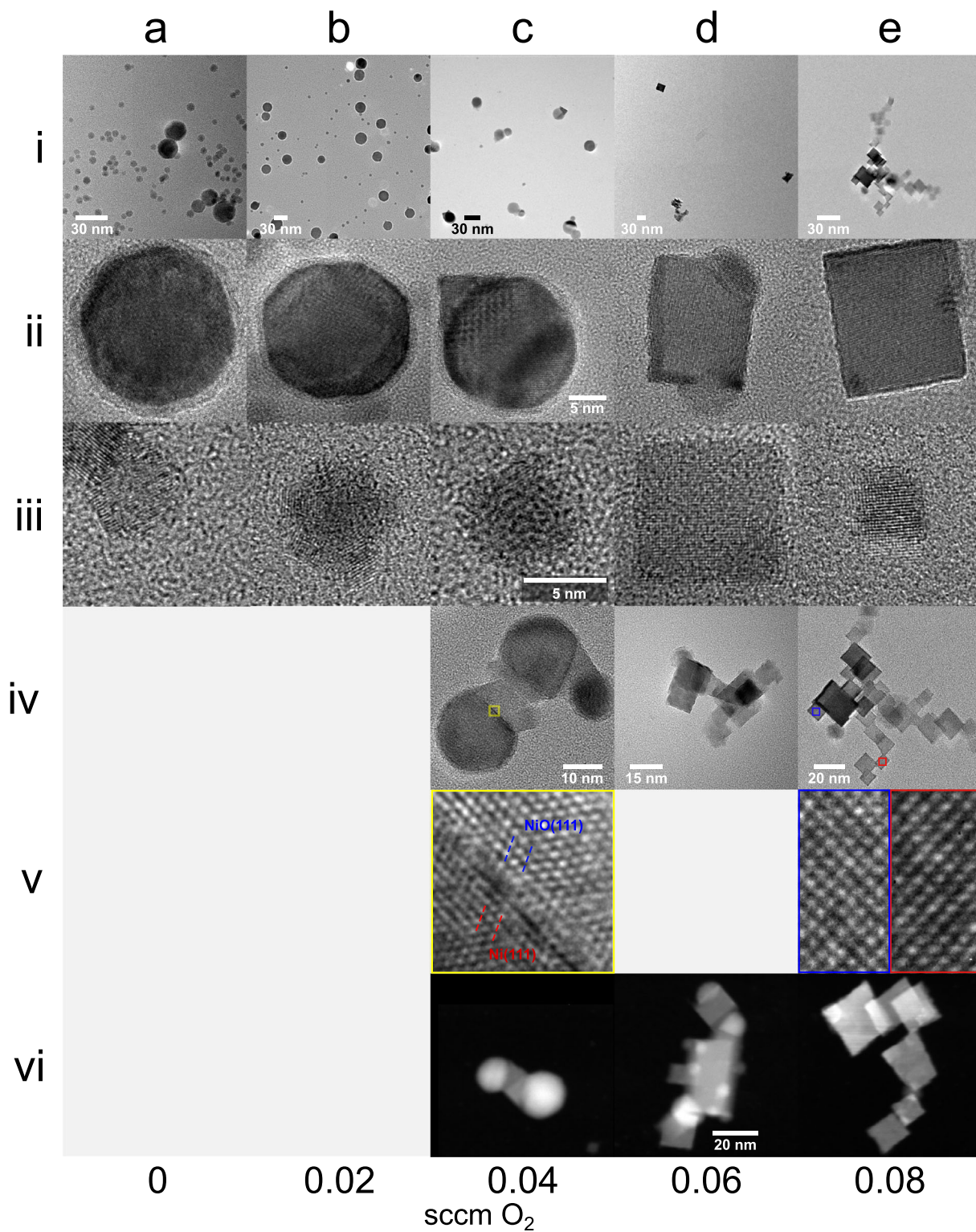


Fig. 2 TEM and STEM HAADF images of the investigated nanoparticles. Columns showing results from the five different investigated O_2 flow rates and rows showing similar phenomena at the different O_2 flows rates: (i) overview, (ii) large nanoparticles,

(iii) smaller nanoparticles, (iv) assemblies, (v) crystal orientation, and (vi) STEM HAADF images. If there is only one scale bar in a row, it applies to all images in the row

At 0.06 sccm and especially at 0.08-sccm O_2 flows, very large assemblies with several tens of crystals are observed (Fig. 2d,iv and e,iv, respectively). Figure 2e,v shows two HRTEM images at different regions of Fig. 2e,iv particle zoomed in areas indicated by color. The analysis of these (and several more spots, not shown) reveals the same crystal orientation throughout the whole assembly. STEM HAADF images (row vi) reveal that between many of the cubic NiO-crystals, there are spherically Ni particles or Ni particles forming sections of a sphere that act as a connection point between individual NiO crystals. These Ni particles are seen more often for the 0.06-sccm case than for the 0.08 sccm one.

XRD has also been used to confirm the existence of the two different phases in the particles presented in Fig. 2. The data agrees with the results above, i.e., that the amount of NiO phase increases and the amount of Ni phase decreases with higher O_2 flows. The XRD results can be found in Supplementary information, Fig. S2.

For O_2 flow rates higher than 0.08 sccm, the process becomes unstable, with arcing as the result. This is due to the formation of insulating oxide layers formed on the cathode surface.

Discussion

Nanoparticles are not likely to form in the very hot environment (1000 to 1500 K (Quesnel et al. 2010; Kashtanov et al. 2010)) inside the hollow cathode but will nucleate as the gas temperature drops in the expanding gas that exits the hollow cathode into the vacuum chamber. As the nanoparticles travel with the gas, they and the gas will be cooled due to expansion and heat exchange with the surrounding gas and will finally reach a temperature close to that of the chamber walls (Hasan et al. 2013; Kashtanov et al. 2010). During this travel, the nanoparticles will grow to their final size by addition of atoms and ions. Aggregation of clusters into larger particles is also possible, but unlikely as the nanoparticles become negatively charged and repel each other when larger than ~ 10 nm in size (Lieberman and Lichtenberg 2005). The partial pressure of oxygen gas will also vary as the nanoparticle pass through the growth zone of the chamber. The main flow in the chamber is the Ar gas streaming through the hollow cathode, out into the chamber, and through the chamber towards the vacuum pump. Oxygen is released

downstream from the growth zone in the lower part of the chamber, and some of the oxygen will diffusively move upstream towards the hollow cathode. This creates a composition gradient that is further strengthened by the fact that oxygen is consumed by the reaction with Ni on the particles. See Fig. 1 for a schematic drawing of the system setup.

The growth conditions are difficult to quantify but will vary with distance away from the hollow cathode and with time. We can, however, qualitatively discuss the growth conditions subjected to the nanoparticles. Assuming steady state conditions, which of course is a bold assumption in a pulsed plasma, the nanoparticle temperature T_{NP} and the partial pressure of oxygen P_{O_2} will vary with unknown functions f and g of the distance z from the cathode exit. We can have some idea of the start and end values of these functions. $T_{NP} = f(z)$ where $f(0 \text{ mm}) \sim 1000 - 1500 \text{ K}$, $f(40 \text{ mm}) \sim 300 - 400 \text{ K}$, and $P_{O_2} = g(z)$, where $g(0 \text{ mm})$ has a very low value and $g(40 \text{ mm})$ has a value that scales with the oxygen gas flow Q_{O_2} , which is the control parameter in these experiments. It is likely, but unknown to us, that Q_{O_2} will influence the function $f(z)$. The speed v_{NP} with which the nanoparticle traverses the growth region, and the deposition rate of Ni atoms and ions onto the nanoparticle $R_{Ni, NP}$ will also be strongly dependent on z , with high values for small z and rapidly decreasing for increasing z . In conclusion, the growth environment for the nanoparticles starts with a very high $R_{Ni, NP}$ and a high T_{NP} . As the nanoparticles proceed through the system, they grow in size, T_{NP} drops, and there is a shift towards more O_2 in the flux to the nanoparticle surface.

It is well known that the formation of oxides on a Ni surface critically depends on P_{O_2} and temperature (Hildebrandt et al. 2000; Kamada et al. 2008), with a thin layer forming at low temperatures and a full oxidation of the Ni crystal at high enough temperature and P_{O_2} . The Ni-O phase diagram shows that (below $\sim 1700 \text{ K}$), there exists only two phases, Ni and NiO (Kowalski and Spencer 1995). In the case of Koga et al., the oxidation is shown to take place not only at $400 \text{ }^\circ\text{C}$ and $P_{O_2} = 533 \text{ Pa}$ but also at $900 \text{ }^\circ\text{C}$ and 1.6 Pa (Koga and Hirasawa 2013). These numbers can be compared with the present work where 0.08 sccm results in $P_{O_2} = 0.2 \text{ Pa}$, if an ideal gas mixture is assumed. However, as mentioned before, there exist a gradient $g(z)$ of the P_{O_2} .

With no O₂ added to the process, pure Ni particles are synthesized. The thin oxide layer is formed when the nanoparticles are exposed to the ambient. Introducing 0.02 sccm of oxygen, Ni nanoparticles are still formed without noticeable more NiO. This indicates that the amount of O₂ introduced to the system is not sufficient to give a high enough P_{O_2} in the growth region, and therefore, no NiO phases will form on the nanoparticles. Earlier studies of similar systems have shown that a small amount of O₂ can aid in the nucleation and initial growth of nanoparticles (Gunnarsson et al. 2018) with a negligible amount of overall oxidation of the nanoparticles (Ekeröth et al. 2018).

Increasing the oxygen flow to 0.04 sccm pushes the process into a growth regime similar to the one described by Hildebrandt et al. (2000). In their case, the Ni surfaces were exposed to an oxygen dose of 25 L, and they observe formation of triangular NiO(111) islands on Ni(111) layer on terraces and parallel to step edges. These equilateral triangular islands are proposed, by Koga and Hirasawa (2013), to be the starting point for the NiO nanorod growth seen in their work. There, the initial NiO crystal consists of a cube corner with a (111) facet in contact with an almost spherical Ni particle. The NiO crystal increases in size until the (111) facet of the NiO reaches a size similar as that of the Ni nanoparticle diameter. When this size is reached, the NiO continues to grow along one of the {100} planes, transforming the cube corner into a rectangularly shaped nanorod. This is due to the fact that NiO growth takes place at the Ni/NiO interface from oxygen dissolved in the Ni crystal (Koga and Hirasawa 2013). In spite of the fact that the phase diagram shows no solubility of oxygen in Ni, considerable amount of oxygen can be dissolved in the near-surface regions at elevated temperatures, >200 °C, and its diffusion rate is significantly higher in this region compared with that in bulk (Deckers et al. 1990; Kortan and Park 1981; Holloway and Outlaw 1981). There is an apparent similarity between results obtained by Koga et al. and the result in the present work. The difference is that they expose O₂ to already made Ni particle, while we expose the nanoparticles to both Ni and O₂ as they grow. As Ni atoms arrive at the surface of a NiO crystal, they can potentially contribute in growing NiO if free O is present.

Alternatively, the Ni atoms can diffuse over the NiO surface reaching the Ni part of the nanoparticle or in the case the Ni atom density is sufficiently high, nucleate as Ni islands on the NiO surface. Thus, new domains of Ni or NiO crystals can nucleate on the existing nanoparticles.

Figure 3 demonstrates a possible path reaching to the structure shown for the highest O₂ flow rates (column e of Fig. 2), using the characteristic features of the nanoparticles as observed for lower flow rates, i.e., we presume that nanoparticles grown using lower oxygen flow can be viewed as snap-shots similar but not identical to particles on the path leading to the assembled nanoparticle structures shown in Fig. 2ii,e, iv,e, and vi,e. The Ni phase is here represented by a darker color and NiO by a lighter color. At 0.04 sccm, several different structures can be observed from small NiO crystals just starting to grow on the Ni nanoparticle to structures with one or several larger NiO crystals and even new Ni crystals formed on the NiO crystal surfaces. At an oxygen flow of 0.06 sccm, the structures consist of larger NiO crystals often connected via a presumably shrinking Ni phase, finally leading to the situation observed at 0.08-sccm oxygen, where the Ni phase has been almost fully consumed and the NiO crystals connect directly to each other. In this process of joining NiO crystals to each other coupled with the simultaneous nucleation and growth of both Ni and NiO, we believe that the mechanism generating the highly oriented assemblies of many NiO crystals is observed for the highest oxygen flows studied.

The assemblies of Ni and NiO phases vary significantly in number of crystals. At the intermediate flow rate, 0.04 sccm, the assemblies consist of both Ni and NiO crystals, with a total number of crystals in a single particle typically ≤ 5 . At higher flow rates, the amount of Ni phase decreases as seen for single crystals, but the number of crystals in an assembly increases with the largest assemblies seen containing up towards 30 NiO crystals in a single assembly. Such an assembly can be seen in Fig. 2e,i. The reason for such a difference in number of crystals in an assembly may be that the time it takes for nanoparticles to travel through the growth zone varies depending

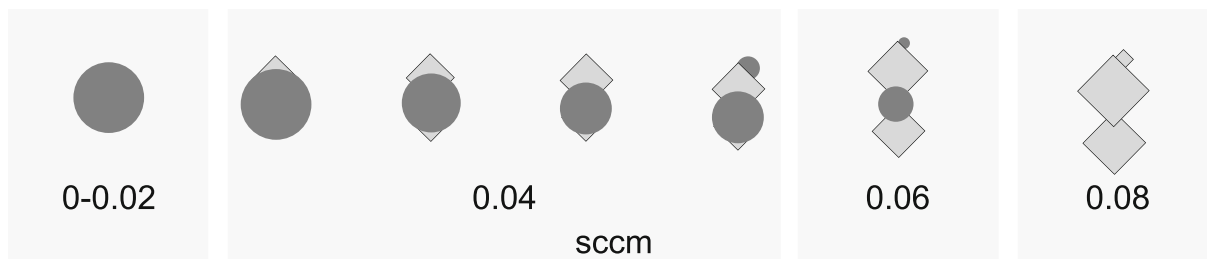


Fig. 3 Schematic illustration of the nanoparticles found and their growth conditions in terms of O_2 flow. For the 0.04-sccm case, the

on the individual paths. Pilch et al. (2013) discussed in a similar way, for the appearance of bi-modal size distributions of nanoparticles, that there are regions with different electric potentials that can either speed up or slow down the nanoparticles on their way through the growth regime. Another possible explanation is that at higher O_2 flow rates, the generation of assemblies starts earlier, closer to the cathodes, since the P_{O_2} is increased and both oxygen and nickel are needed for the assemblies to form.

Conclusion

This work shows that it is possible to controllably grow dual-phase Ni/NiO nanoparticles with varying phase compositions using the high-power pulsed hollow cathode sputtering technique. The level of oxidation is controlled through the regulation of the amount of oxygen flow introduced into the chamber. The grown particles range from pure Ni nanoparticles with a native oxide shell, through dual-phase particles containing both Ni and NiO to fully oxidized NiO nanoparticles. Large assemblies of nanoparticles with their crystal lattices aligned are formed at the higher oxygen flows investigated. This results in a large number of Ni/NiO crystal interfaces. A mechanism for the assembly formation is suggested and is a result of simultaneous arrival of both Ni and O atoms at the surface of the growing particle.

Funding information This work was made possible by the financial support from the Knut and Alice Wallenberg Foundation (KAW 2014.0276) and support from the Swedish Government Strategic Research Area in Materials Science on Functional Materials at Linköping University (Faculty Grant SFO Mat LiU No. 2009 00971). SI and TS would like to acknowledge support from the Tokyo Metropolitan University in the framework of Co-tutorial Program with Linköping University.

evolution of NiO crystals as well as nucleation of new Ni islands on the NiO surface are also displayed

Compliance with ethical standards

Conflicts of interest The authors declare that there are no conflicts of interest.

Publisher's note Springer Nature remains neutral with regard to jurisdictional claims in published maps and institutional affiliations.

References

- Bartel LC, Morosin B (1971) Exchange striction in NiO. *Phys Rev B* 3:1039–1043
- Bell J, Ye R, Ahmed K, Liu C, Ozkan M, Ozkan CS (2015) Free-standing Ni-NiO nanofiber cloth anode for high capacity and high rate Li-ion batteries. *Nano Energy* 18:47–56
- Cheng N, Stambula S, Wang D, Banis MN, Liu J, Riese A, Xiao B, Li R, Sham T-K, Liu L-M, Botton GA, Sun X (2016) Platinum single-atom and cluster catalysis of the hydrogen evolution reaction. *Nat Commun* 7:13638
- Deckers S, Habraken FHPM, van der Weg WF (1990) Oxidation of clean and Pt-covered Ni (111). *Appl Surf Sci* 45:207–220
- Ekeröth S, Münger EP, Boyd R, Ekspong J, Wågberg T, Edman L, Brenning N, Helmersson U (2018) Catalytic nanotruss structures realized by magnetic self-assembly in pulsed plasma. *Nano Lett* 18:3132–3137
- El-Kemary M, Nagy N, El-Mehasseb I (2013) Nickel oxide nanoparticles: synthesis and spectral studies of interactions with glucose. *Mater Sci Semicond Process* 16:1747–1752
- Gang Wu Z, Munoz M, Montero O (2010) The synthesis of nickel nanoparticles by hydrazine reduction. *Adv Powder Technol* 21:165–168
- Gong M, Zhou W, Tsai M-C, Zhou J, Guan M, Lin M-C, Zhang B, Hu Y, Wang D-Y, Yang J, Pennycook SJ, Hwang B-J, Dai H (2014) Nanoscale nickel oxide/nickel heterostructures for active hydrogen evolution electrocatalysis. *Nat Commun* 5:4695
- Gunnarsson R, Brenning N, Boyd RD, Helmersson U (2018) Nucleation of titanium nanoparticles in an oxygen-starved environment. I: experiments. *J Phys D Appl Phys* 51:455201
- Hasan MI, Pilch I, Söderström D, Lundin D, Helmersson U, Brenning N (2013) Modeling the extraction of sputtered metal from high power impulse hollow

- cathode discharges. *Plasma Sources Sci Technol* 22: 035006
- Hildebrandt S, Hagendorf C, Doege T, Jecksties C, Kulla R, Neddermeyer H (2000) Real time scanning tunneling microscopy study of the initial stages of oxidation of Ni(111) between 400 and 470 K. *J Vac Sci Technol A* 18:1010–1015
- Holloway PH, Outlaw RA (1981) The effects of temperature upon NiO formation and oxygen removal on Ni(110). *Surf Sci* 111: 300–316
- Jesús JC, Pereira P, Carrazza J, Zaera F (1996) Influence of argon ion bombardment on the oxidation of nickel surfaces. *Surf Sci* 369:217–230
- Jian J, Shi Y, Ekeröth S, Keraudy J, Syväjärvi M, Yakimova R, Helmersson U, Sun J (2019) Nanostructured NiO/cubic SiC p-n heterojunction photoanode for enhanced solar water splitting. *J Mater Chem A*. Accepted Manuscript
- Kamada T, Sogo M, Aoki M, Masuda S (2008) Mesoscopic pattern formation during initial oxidation of Ni(111) observed by electron emission microscopy. *Surf Sci* 602:724–732
- Kashtanov PV, Smirnov BM, Hippler R (2010) Efficiency of cluster generation in a magnetron discharge. *EPL Europhys Lett* 91:63001
- Kittel C (1996) Introduction to solid state physics, 7th edn. John Wiley & Sons, Inc., Hoboken, p 23
- Koga K, Hirasawa M (2013) Anisotropic growth of NiO nanorods from Ni nanoparticles by rapid thermal oxidation. *Nanotechnology* 24:375602
- Kortan AR, Park RL (1981) Phase diagram of oxygen chemisorbed on nickel (111). *Phys Rev B* 12:6340
- Kowalski M, Spencer PJ (1995) Thermodynamic reevaluation of the Cr-O, Fe-O and Ni-O systems: remodelling of the liquid, bcc and fcc phases. *Calphad* 19:229–243
- Lieberman MA, Lichtenberg AJ (2005) Principles of plasma discharges and materials processing, 2nd ed., Chap. 17.4. John Wiley & Sons, Hoboken, New Jersey, pp 662–668
- Liu F, Wang X, Hao J, Han S, Lian J, Jiang Q (2017) High density arrayed Ni/NiO core-shell nanospheres evenly distributed on graphene for ultrahigh performance supercapacitor. *Sci Rep* 7:17709
- Pan X, Zhou G (2018) A theoretical study on the mechanism of hydrogen evolution on non-precious partially oxidized nickel-based heterostructures for fuel cells. *Phys Chem Chem Phys* 20:7968–7973
- Park J-W, Altstetter CJ (1987) The diffusion and solubility of oxygen in solid nickel. *Metall Trans A* 18:43–50
- Pilch I, Söderström D, Brenning N, Helmersson U (2013) Size-controlled growth of nanoparticles in a highly ionized pulsed plasma. *Appl Phys Lett* 102:033108
- Quesnel E, Pauliac-Vaujour E, Muffato V (2010) Modeling metallic nanoparticle synthesis in a magnetron-based nanocluster source by gas condensation of a sputtered vapor. *J Appl Phys* 107:054309
- Spadaro MC, Addato SD, Luches P, Valeri S, Grillo V, Rotunno E, Roldan MA, Pennycook SJ, Ferretti AM, Capetti E, Ponti A (2015) Tunability of exchange bias in Ni@NiO core-shell nanoparticles obtained by sequential layer deposition. *Nanotechnology* 26:405704
- Subbaraman R, Tripkovic D, Strmcnik D, Chang K-C, Uchimura M, Paulikas AP, Stamenkovic V, Marcovic NM (2011) Enhancing hydrogen evolution activity in water splitting by tailoring Li⁺-Ni(OH)₂-Pt interfaces. *Science* 334:6060
- Wang J, Mao S, Liu Z, Wei Z, Wang H, Chen Y, Wang Y (2017) Dominating role of Ni⁰ on the interface of Ni/NiO for enhanced hydrogen evolution reaction. *ACS Appl Mater Interfaces* 9(8):7139–7147
- Yeh Y-H, Yu T-Y, Liu M-C, Cheng Y-J (2017) Enhanced water splitting performance of GaN photoanode using self-assembled nickel/nickel-oxide nanoparticle catalyst. *Int J Hydrog Energy* 42:27066–27072
- Yin H, Zhao S, Zhao K, Muqsit A, Tang H, Chang L, Zhao H, Gao Y, Tang Z (2015) Ultrathin platinum nanowires grown on single-layered nickel hydroxide with high hydrogen evolution activity. *Nat Commun* 6:6430
- Yung T-Y, Huang L-Y, Chan T-Y, Wang K-S, Liu T-Y, Chen P-T, Chao C-Y, Liu L-K (2014) Synthesis and characterizations of Ni-NiO nanoparticles on PDDA-modified graphene for oxygen reduction reaction. *Nanoscale Res Lett* 9:444